CHARACTERIZATION OF CURRENT SHEET EVOLUTION IN A PULSED ELECTROMAGNETIC ACCELERATOR[*]

J.W. Berkery[†]and **E.Y. Choueiri**[‡]
Electric Propulsion and Plasma Dynamics Laboratory
Princeton University, Princeton, New Jersey 08540

March 17-21, 2003

Abstract

A detailed experimental characterization of current sheet evolution in a pulsed electromagnetic accelerator is presented based on temporally and spatially resolved measurements of the magnetic field in the device. The dynamics of current sheets generally depart from the ideal snowplow dynamics and are consequently associated with various non-idealities. Magnetic probes (B-dot probes) were used at 432 spatial locations in the device to obtain a description of the magnetic field evolution. The corresponding current sheet evolution was abstracted from the magnetic field data and shows a complex structure of the current sheet during the initial part of its evolution. The measurements show the current sheet evolves from a sheet perpendicular to the electrodes to a structure exhibiting a main trunk and a canted branch near the anode. The canted branch evolves into a final canted current sheet front, short circuiting the trunk and leaving it behind in its wake. These observed features are in good agreement with the phenomenological description derived previously from a photographic survey of the discharge. The magnetic field measurements compliment the previous photographic survey as the latter indicates the location of the discharge (through filtered ion emission) but cannot show directly where the current sheet is located. While the magnetic field measurements can provide an unambiguous picture of the current location, they do not show where all of the plasma is.

1 Introduction

Gas-fed pulsed plasma thrusters utilize a current sheet to accelerate gas and produce thrust. The ideal snowplow model of current sheet propagation in these devices describes the sheet as an impermeable plasma sheet that entrains and accelerates all of the neutral gas it encounters [1]. It has often been observed that the sheet does not behave in this ideal manner [6], [8], [11], [10]. Non-ideality in the current sheet propagation can lead to a decrease in performance of the thruster [2].

Two major non-idealities have been previously identified: current sheet canting and current sheet permeability. Current sheet canting is the tendency of the sheet to deviate from perpendicularity to the electrodes; it has been studied in detail by Markusic and Choueiri [3], [4]. Canting of the current sheet could lead to the undesired effect of an off-axis thrust vector.

Current sheet permeability is the tendency of the sheet to allow neutral or ionized gas to slip behind it, in a variety of ways. These include the penetration of neutrals directly through the sheet and the slippage of ions behind the sheet at the cathode [5]. Although researchers have identified evidence of permeability of current sheets, the topic has not been explored in detail [6], [7], [8], [9], [11], [10]. Current sheet permeability can lead to lowered mass utilization efficiency, and loss of momentum in the plasma, leading to lowered thrust.

A previous photographic survey, along with limited magnetic and interferometric measurements (measurements were made in only a few locations) has lead to a phenomenological description of the current sheet evolution [4]. According to this description the sheet initially forms as an ideal sheet, but soon a branch of plasma runs along the anode, ahead of the initial trunk. This leads to the canted structure, because the branch soon cuts off the trunk from conducting current and effectively becomes the current sheet, with the anode attachment out in front of the cathode attachment. The trunk and branch are visible in figure 1a, which is taken $3\mu s$ into the discharge. After $5\mu s$ (figure 1b) the canted structure is fully formed and continues at essentially the same canting angle downstream in the thruster.

Photographic evidence suggests that the trunk falls behind the new branch sheet, and could become part of what has been identified as a plasma wake or bubble. This wake continues to move at a slower rate than the sheet, falling further behind. This wake has been identified as a bubble or hook structure in the past, and indeed looks similar to a hook in figure 1b and a bubble $5\mu s$ later, in figure 1c. We have previously determined, through interferometry, that the electron density in the wake is significant compared to that in the sheet [5]. It remains to be confirmed, however, that the disconnected trunk is indeed the origin of the plasma wake.

At later times, when the sheet has separated itself from the slower-moving wake, a trail of plasma along the cathode is also left behind. A
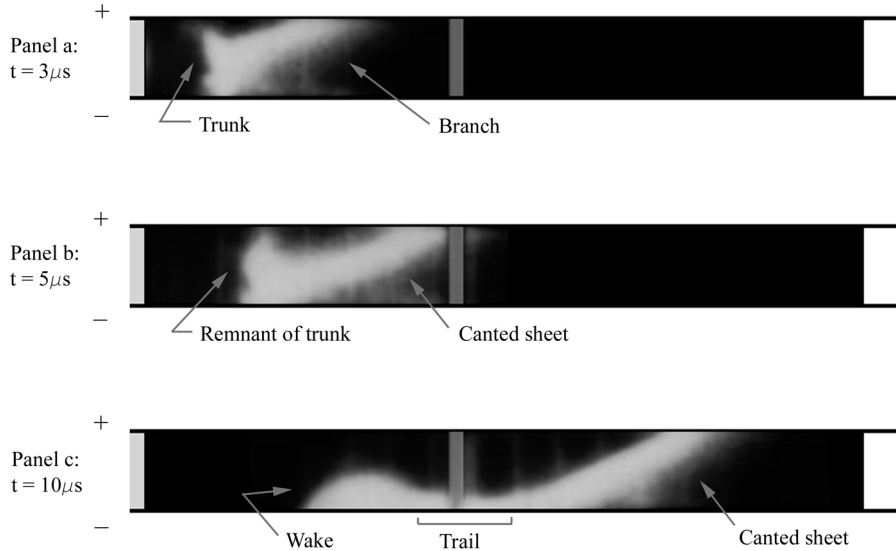
Figure 1: Photograph of the discharge at $t = 3, 5$, and 10 μ s. (The vertical grey object at the left of the accelerator is an insulator backplate, and at the center is a post that blocked the camera.) From reference [12].

possible source of this plasma trail may be ions which are directed towards the cathode by the skewed $j \times B$ force density of the canted sheet.

The initial development of the branch and trunk structure of the sheet, described by Markusic and Choueiri [4], is based mostly on photographic evidence. While these photographs show where the plasma is located in the device, the question remains whether the plasma location is the same as where the current flows. To answer that question we present detailed magnetic field measurements obtained with time resolution in a spatial grid inside the accelerator. These magnetic field measurements allow the determination of the current density pattern in the electrode gap with spatial and temporal resolution. By comparing these photographic, magnetic and current density data, we obtain a complimentary description of the current sheet evolution which is supportive of the phenomenological description.

2   Description of the Apparatus

The device used in this experimental study is the same as that used by Markusic in his current sheet canting studies. It is described in detail in reference [3], but will be briefly described here as well. It is a parallel plate accelerator with glass sidewalls and was constructed with ease of diagnosis in mind. The anode and cathode are made of copper and the area of the
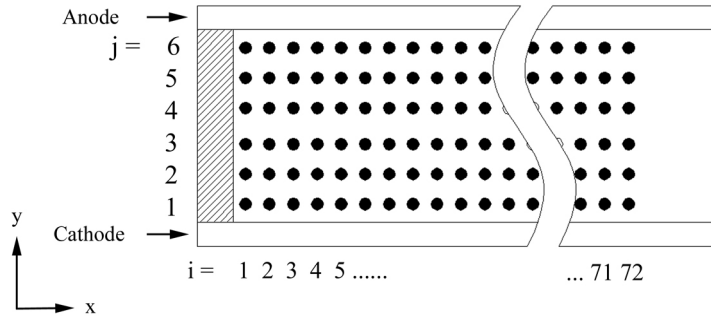
Figure 2: The array of measurement points in the accelerator is shown. The top copper plate is the anode, the bottom plate is the cathode. An insulator backplate is shown (shaded). The coordinate system is also defined. Note that the z direction is out of the page.

acceleration region measures 60.96 cm long and 10.16 cm wide, with a gap of 5.08 cm between the plates. The propellant is uniformly filled in the acceleration region by filling the entire vacuum vessel to the desired pressure.

The current sheet is formed in this device through a pulse forming network consisting of ten stages of 10 μF capacitors and 100 nH inductors. The device is triggered by an ignitron. A typical current pulse [3] resulting from a 9 kV applied voltage is a fairly flat current of about 60 kA lasting approximately 25 μs, with a rise time on the order of 2 μs.

3   Magnetic Field Measurements

The need for more information about the evolution of the current sheet, especially at early times, is clear. To this end, we present results from a study using B-dot probes. The probes are coils on which a voltage is induced that is proportional to the time variation of the magnetic field. These probes are also described in detail elsewhere [3]. The 0.25 cm diameter coils are encased in a quartz tube that protects them from the plasma. These tubes, which are inserted into the accelerator from the downstream direction, are 0.318 cm in diameter. The $\dot{B}$ signal which is obtained from these probes is integrated numerically to obtain traces of $B(t)$ at the specific location of the probe.

The quantitative data to be determined from these measurements are twofold. First, the arrival of a steep magnetic field rise at a point will be taken as evidence of the arrival of the current sheet. From this knowledge at many points in the accelerator, the time-resolved velocity of the current sheet may be determined. Second, the value of the magnetic field is resolved
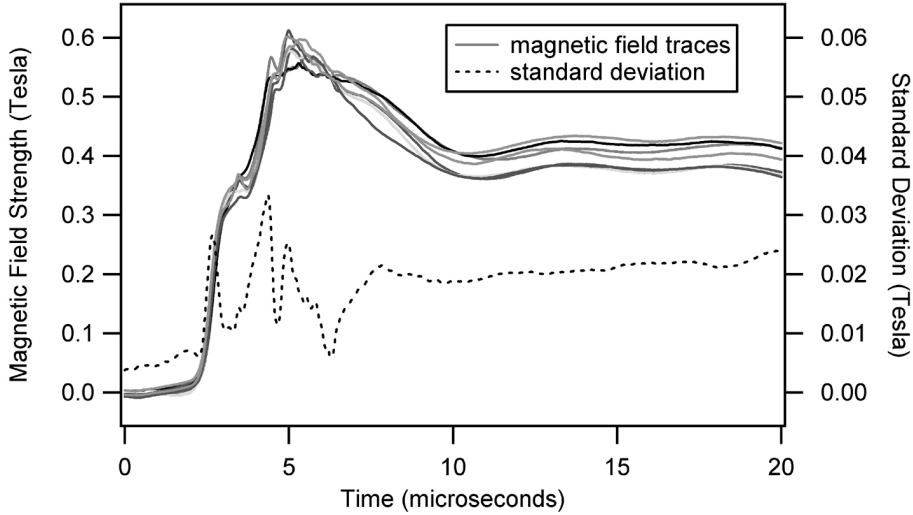
Figure 3: Magnetic field strength versus time for seven separate shots taken at the same physical location. The standard deviation of the seven measurements is also shown (dashed) on the right axis. The probe was located at position (12,4).

at different locations in the accelerator. This also allows the determination the current density contours during the acceleration. Perhaps the most valuable information we can obtain from the magnetic field measurements is a clear picture of the development of structures in the current sheet at early times.

Time resolved measurements of dB/dt were made over a grid of points covering the inter-electrode space, as shown in figure 2. This array of data points consisted of 6 vertical locations by 72 horizontal locations. The horizontal spacing (x direction) was constant at 0.635 cm, with an uncertainty of plus or minus 0.159 cm. This uncertainty is due to the ability of a translation device used to move the probes to accurately position the tips. Vertically (y direction), the data points were spaced at the following distances from the cathode (the bottom electrode) in the 5.08 cm gap: 0.476 cm, 1.270 cm, 2.064 cm, 3.016 cm, 3.810 cm, and 4.604 cm, with an uncertainty of plus or minus 0.318 cm, the diameter of the quartz tubes in which the coils are housed. The probed locations will be referred to as (i, j), where i and j are the x and y positions as labelled in figure 2. All measurements, unless otherwise specified were taken at the centerline of the thruster in the z dimension.

Measurements have been obtained for one operating condition (argon propellant, 100 mTorr, 9 kV). The photographs presented above were obtained with an argon discharge at 100 mTorr pressure as well, however the
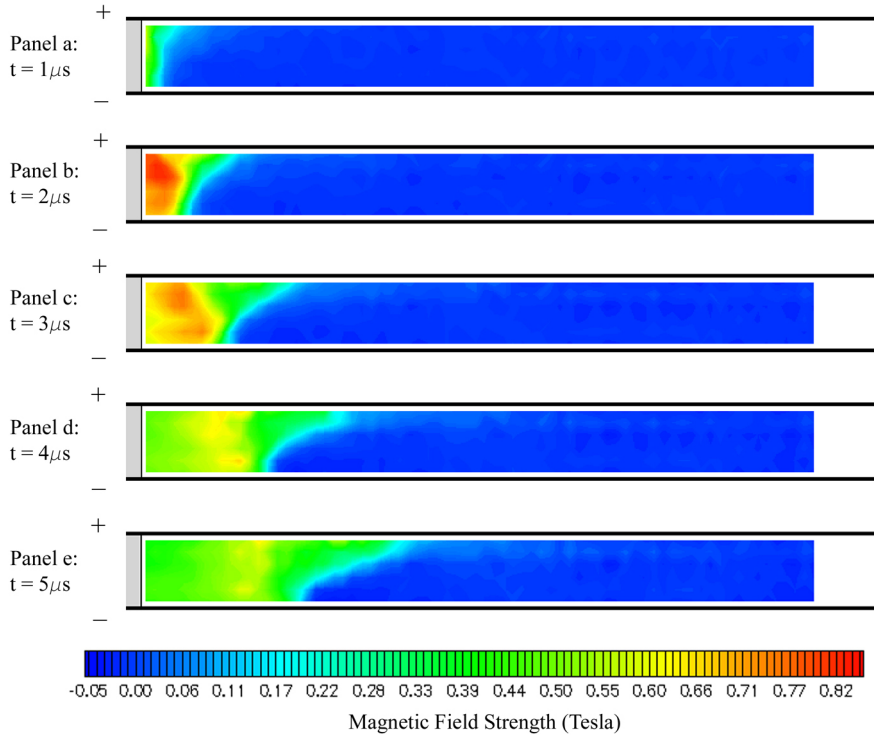
5

Figure 4: Magnetic field contours at $t = 1 - 5\mu s$.

voltage was lower (4 kV compared to 9 kV), and the trigger timing was not the same, thus the photographs presented above and magnetic contours presented later should not be expected to match exactly.

It is important to note that since only two B-dot probes were employed, only two out of the 432 locations were probed during a single discharge. The composite map of the magnetic field was then constructed from data obtained during many discharges. The data was repeatable as is evident by eight tests in which measurements were made six or seven times in a row at the same location and with the same conditions. One example of these repeatability tests is shown in figure 3, which shows seven traces of the B field obtained from directly integrating the $\dot{B}$ traces from seven discharges repeated at the same conditions. These traces are typical examples of the data that was collected.

From these repeatability tests we were able to determine the standard deviation of the measurements which was plotted using the right axis in figure 3. The inaccuracy of the probes is very small (less than 1%) as verified by calibration with a Helmholtz coil [3]. Most of the error is due to the standard deviation of the repeatability. The highest standard deviation found in all of the repeatability tests was 0.05 Tesla, or approximately 10%.
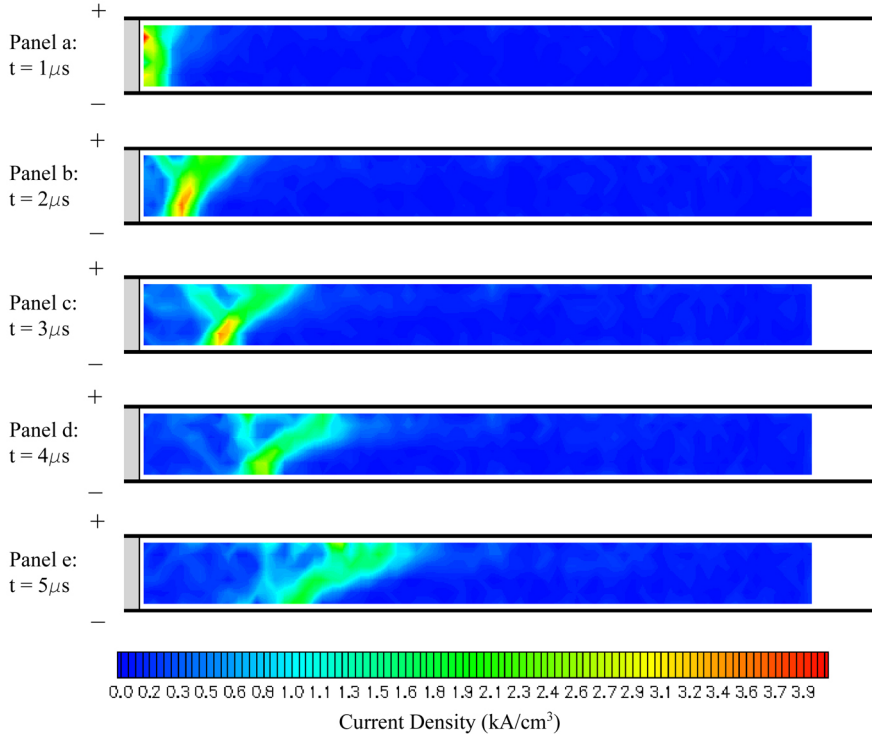
Figure 5: Current density contours at $t = 1 - 5\mu s$.

With this method, at any given time in the discharge, the value of the magnetic field is known at 432 physical locations. From this knowledge, a contour plot can be constructed. This is done by displaying the magnetic field strength with a range of colors, as shown in figure 4. Due to the smoothing in between the grid points, any structure observed that is less than the grid spacing of figure 2 should not be interpreted as physical. This method provides a vivid visual display of the evolution of the magnetic field with time.

A movie [13] has been generated from seventy frames such as those shown in figure 4. With a spacing of $0.2\mu s$ between frames, the movie contains 70 frames, covering $14\mu s$ of the discharge.

4   Current Density Contours

If we consider the dimension in which the current sheet propagates to be $\hat{x}$ and the vertical dimension to be $\hat{y}$, then the magnetic field is in the $-\hat{z}$ direction. In this case, the total current density can be found from $\nabla \times \vec{\mathbf{B}} = \mu_0 \vec{\mathbf{j}}$, which for our particular configuration yields the following expression for the current density:
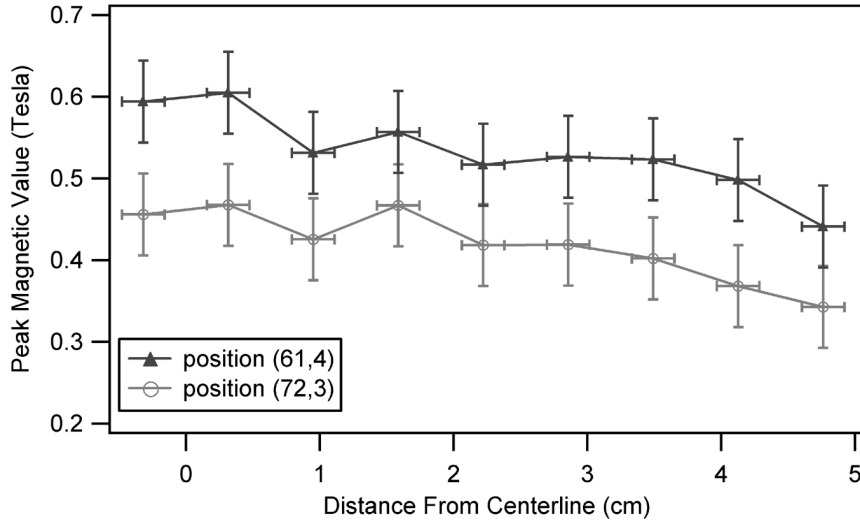
Figure 6: Peak magnetic field values vs. distance from the center in the z dimension for two different (x,y) positions. The error in the magnetic field measurement is taken as the largest standard deviation from repeatability tests, as discussed in section 3.

$$ j = \frac{1}{\mu_0}[(-\frac{dB}{dx})^2 + (\frac{dB}{dy})^2]^{\frac{1}{2}} \qquad (1) $$

This expression is then evaluated over the grid to yield a temporally and spatially resolved contour plot of the current density.

There are two limitations with this technique. First, the assumption that the magnetic field is constant in the transverse (z) direction, which simplifies the evaluation of equation 1 was found to not be entirely correct. Figure 6 shows that there is a drop-off of approximately 25% in the peak magnetic field strength from the center to the side in the z dimension.

The fact that the electrodes are separated by 5.08 cm in the y direction and are 10.16 cm wide in the z direction gives an aspect ratio of 1:2. Some deviation from ideal, straight and constant magnetic fields should be expected then. This magnetic flux leakage can cause inefficiency in the $j \times B$ acceleration [14].

Furthermore, there is an error associated with taking the finite differences of the discrete data while evaluation equation 1. However, the resulting plots are still insightful because they allow a visualization of the current pattern and its evolution. Quantitatively, the current density contours are expected to be essentially correct. Examples of such plots are shown in figure 5 at the same points in time as the magnetic field contours previously shown in figure 4. A movie [13] was generated from the resulting frames as was done for the case of magnetic field contours.

8

5 Discussion

The magnetic field contours that have been obtained are insightful, particularly in confirming the phenomenological description of the early stages of the development of the current sheet. Several major features or trends are recognizable. The first is that the sheet, defined by the sharp gradient in magnetic field, begins as a planar sheet that is perpendicular to the electrodes, but soon begins to cant (figure 4a). The magnetic field near the anode moves at a faster speed and branches away from the trunk of the sheet (figure 4b). At the same time, a region of higher magnetic field can be seen trailing the sheet (figure 4b and 4c). While the sheet is establishing its fully developed canting angle, the trailing region of higher magnetic field begins to fade (figure 4d). By 5 μs the field structure has reached a fairly constant pattern (figure 4e). Downstream of the sheet the magnetic field strength is zero and upstream of the sheet, the field is fairly constant at approximately 0.4 Tesla. The sheet remains at a constant canting angle as it propagates from this time on.

The velocity of the current sheet can be obtained from these contour plots as well. If we take a rise from 0 to 0.2 Tesla as evidence of the arrival of the sheet, we find that near the anode the sheet travels at a fairly constant speed of about 4 cm/μs. Near the cathode, the sheet starts at about 2 cm/μs and increases in velocity to 4 cm/μs until the velocity is nearly constant everywhere by about 6 μs. This is consistent with the conclusions drawn above, that the branch speeds ahead of the trunk at a higher velocity and that the canting angle is constant after an initial period.

The features identified here as a branching magnetic field which pushes ahead and a region of higher magnetic field which lags behind support the phenomenological description in reference [4] on the basis of more limited magnetic evidence, as well as interferometry and high speed photography. We can see even more clearly from the current density contours that these structures are the same plasma columns that were previously identified in that study as the branch and trunk.

Figure 5 clearly shows two paths of current attaching to the anode at 2 and 3 μs. After another 2 μs (figure 5e) the trunk has ceased to carry current. At this time the branch has become the canted current sheet, and the trunk has become a body of plasma behind the sheet that does not carry current. The trunk will no longer feel a $j \times B$ force density, and will continue at a lower speed than the sheet due to its inertia. From photographs [12], it can be determined that the velocity of the wake is fairly constant ($\sim$ 1.5 cm/μs) and close to the initial velocity of the trunk ($\sim$ 2 cm/μs). This is consistent with the deduction that the wake is the remnant of the trunk.

The question arises whether the trunk remains a plasma after it ceases to carry current. Three-body recombination is likely to be the important process for plasma decay. From Raizer [15], we can estimate the three-body

recombination time scale as:

$$\tau_{tbr} = \frac{1.14 \times 10^{26} * (T_i)^{4.5}}{(n_e)^2} \tag{2}$$

Here the ion temperature is in units of eV and electron density is in units of cm^{-3}.

From previous measurements we know the peak electron number density in the wake (for the conditions of this study, argon, 100 mTorr) is approximately 3×10^{15} cm^{-3} [5]. The measured electron temperature in the current sheet is 2.4 eV [3], but the ion temperature in the wake is not known. Thus, if the wake plasma is expected to persist on the same time scale as its lifetime in the device, ~ 14 μs, we find from the above equation that the ion temperature must be greater than about 1 eV, which is not unreasonable. From photographic evidence it appears that the plasma does persist, although it may be continually replenished from the plasma trail.

6 Conclusions

A detailed experimental characterization of current sheet evolution based on temporally and spatially resolved measurements of the magnetic field in a pulsed electromagnetic accelerator has been presented. The magnetic field measurements have also been used to construct current density contours, which show the location of the current sheet in the device. This information compliments previous photographic surveys which indicated the location of the plasma but cannot directly show where the current flows. The measurements show the early development of the current sheet from a ideal planar sheet to a more complicated structure consisting of a trunk and a canted branch near the anode. The canted branch evolves into the canted current sheet, while the trunk ceases to carry current and is left behind as a plasma wake. These observed features are in good agreement with the previously presented phenomenological description. Unanswered questions about the development of plasma structures in this accelerator remain, however. These include:

- How much plasma is contained in the sheet, and what percent slips into the wake and the trail?

- What is the mechanism for plasma leakage at the cathode, forming the plasma trail, and does the trail feed the plasma wake?

- How much momentum is lost by the inefficiencies of the current sheet?

- To what extent do these departures from the ideal snow plow behavior impact the efficiency of the accelerator?

Now that we have a quantitative database of the current sheet evolution in time and space, it can be used to address questions about current sheet permeability. In addition, several other experiments are being planned. The first is an interferometry experiment to provide spatially (in a similar grid to that used in this work) and temporally resolved measurements of the electron number density of the plasma in all of the structures. The second is a spectroscopy experiment to track the movement of neutral atoms that the sheet encounters.

References

[1] P.J. Hart. Plasma acceleration with coaxial electrodes. *The Physics of Fluids*, 5(1):38–47, January 1962.

[2] J.K. Ziemer. *Performance Scaling of Gas-Fed Pulsed Plasma Thrusters.* PhD thesis, Princeton University, 2001.

[3] T.E. Markusic. *Current Sheet Canting in Pulsed Electromagnetic Accelerators.* PhD thesis, Princeton University, 2002.

[4] T.E. Markusic and E.Y. Choueiri. Phenomenological model of current sheet canting in pulsed electromagnetic accelerators. In 28th *International Electric Propulsion Conference*, Toulouse, France, March 17-24 2003. IEPC 2003-0293.

[5] J.W. Berkery and E.Y. Choueiri. Current sheet permeability in electromagnetic pulsed plasma thrusters. In 38th *Joint Propulsion Conference*, Indianapolis, Indiana, July 7-10 2002. AIAA 2002-4120.

[6] L.C. Burkhardt and R.H. Lovberg. Current sheet in a coaxial plasma gun. *The Physics of Fluids*, 5(3):341–347, March 1962.

[7] R.H. Lovberg. The measurement of plasma density in a rail accelerator by means of schlieren photography. *IEEE Transactions on Nuclear Science*, 11:187–198, 1964.

[8] R.H. Lovberg. Investigation of current-sheet microstructure. *AIAA Journal*, 4(7):1215, 1966.

[9] T.M. York and R.G. Jahn. Pressure distribution in the structure of a propagation current sheet. *The Physics of Fluids*, 13(5):1303, 1970.

[10] F.J. Fishman and H. Petschek. Flow model for large radius-ratio magnetic annular shock-tube operation. *Physics of Fluids*, 5:632–633, 1962.

[11] J.C. Keck. Current distribution in a magnetic annular shock tube. *Physics of Fluids*, 5:630–632, 1962.

[12] T.E. Markusic. Movie of a parallel-plate gas-fed pulsed plasma thruster discharge. http://www.princeton.edu/~eppdyl/personnel/markusic.html.

[13] J.W. Berkery. Movies of experimental contours in a parallel-plate gas-fed pulsed plasma thruster discharge. http://www.princeton.edu/~eppdyl/personnel/berkery.html.

[14] I. Kohlberg and W.O. Coburn. A solution for three dimensional rail gun current distribution and electromagnetic fields of a rail launcher. *IEEE Transactions on Magnetics*, 31(1):628–633, 1995.

[15] Y.P. Raizer. *Gas Discharge Physics*. Springer-Verlag, 1991.